

# Towards a long-term record of solar total and spectral irradiance

N. A. Krivova<sup>a</sup>, S. K. Solanki<sup>a,b</sup>, Y. C. Unruh<sup>c</sup>

<sup>a</sup>*Max-Planck-Institut für Sonnensystemforschung, Max-Planck-Str. 2, 37191  
Katlenburg-Lindau, Germany*

<sup>b</sup>*School of Space Research, Kyung Hee University, Yongin, Gyeonggi 446-701, Korea*

<sup>c</sup>*Astrophysics Group, Blackett Laboratory, Imperial College London, SW7 2AZ, United  
Kingdom*

---

## Abstract

The variation of total solar irradiance (TSI) has been measured since 1978 and that of the spectral irradiance for an even shorter amount of time. Semi-empirical models are now available that reproduce over 80% of the measured irradiance variations. An extension of these models into the more distant past is needed in order to serve as input to climate simulations. Here we review our most recent efforts to model solar total and spectral irradiance on time scales from days to centuries and even longer. Solar spectral irradiance has been reconstructed since 1947. Reconstruction of solar total irradiance goes back to 1610 and suggests a value of about  $1\text{--}1.5\text{ Wm}^{-2}$  for the increase in the cycle-averaged TSI since the end of the Maunder minimum, which is significantly lower than previously assumed but agrees with other modern models. First steps have also been made towards reconstructions of solar total and spectral irradiance on time scales of millennia.

*Key words:* solar irradiance, solar magnetic fields, solar-terrestrial relations, solar variability

---

## 1. Introduction

Solar irradiance is the total energy flux (or energy received per unit area and time) at the top of the Earth's atmosphere. It is strongly wavelength dependent: less than 8% of the solar energy is emitted at wavelengths below 400 nm, more than 60% come from the wavelengths between 400 and 1000 nm and roughly another 30% from the longer wavelengths (e.g., Solanki and Unruh, 1998; Krivova et al., 2006).

The small contribution of the UV part of the spectrum is, however, compensated by the spectral dependence of the transmission of the Earth's atmosphere. Thus solar radiation below 300 nm is almost completely absorbed in the atmosphere (see, e.g., Haigh, 2007, and references therein) and is important for the chemistry of the stratosphere and overlying layers. In particular, radiation in the Ly- $\alpha$  line (121.6 nm) and in the oxygen continuum and bands between 180 and 240 nm controls production and destruction of ozone (e.g., Frederick, 1977; Brasseur and Simon, 1981; Haigh, 1994, 2007; Fleming et al., 1995; Egorova et al., 2004; Langematz et al., 2005). Solar UV radiation at 200–350 nm is the main heat source in the stratosphere and mesosphere (Haigh, 1999, 2007; Rozanov et al., 2006).

The role of the solar UV radiation for the Earth's climate is boosted further by the fact that variations of solar irradiance are also strongly wavelength dependent. Whereas the total (integrated over all wavelengths) solar irradiance varies by only about 0.1% over the solar cycle, the UV irradiance varies by 1 to 3 orders of magnitude more (e.g., Floyd et al., 2003).

Solar near-IR radiation absorbed by water vapour and carbon dioxide is an important source of heating in the lower atmosphere (Haigh, 2007). Solar

variability in the IR is comparable to or lower than the TSI variations and in the range between about 1500 and 2500 nm it is reversed with respect to the solar cycle (Harder et al., 2009; Krivova et al., 2009b).

Solid assessment of the solar forcing on the Earth's climate is still plagued, among other factors, by a shortage of reliable and sufficiently long irradiance records. The time series of direct space-borne measurements of solar irradiance is only 3 decades long (in case of spectral irradiance, even shorter). Consequently, models are required to extend the irradiance time series to earlier times. In the last years, considerable advances have been made in modelling the solar total irradiance. Also, spectral models started gathering force. Reconstructions of the past variations are quite accurate for the last decades, when sufficiently high resolution measurements of the solar photospheric magnetic flux (i.e. magnetograms) exist. On longer time scales, the secular trend remains rather uncertain and until very recently the reconstructions were limited to the telescope era, i.e. to the last 4 centuries.

Domingo et al. (2009) have recently presented an overview of different types of irradiance models on time scales of days up to the solar cycle. Here we review the most recent progress in modelling solar total and spectral irradiance on time scales from days to centuries and even longer using the SATIRE set of models. Before discussing the model we briefly describe the available observational data (Sect. 2.1) and main sources of irradiance variations (Sect. 2.2). In Sect. 3 we concentrate on the period when direct irradiance measurements are available, in Sects. 4 and 5 we discuss the reconstructions for the telescope era and the first steps towards longer-term reconstructions, respectively. Section 6 summarises our current knowledge

on irradiance variations on time scales of interest for climate research.

## 2. Solar Irradiance Variations

### 2.1. Observations

#### 2.1.1. Total Solar Irradiance

Measurements of the total solar irradiance (TSI) from space, having sufficient accuracy to detect its variations, started with the Hickey-Frieden (HF) radiometer (Hickey et al., 1980) aboard the NOAA/NASA mission Nimbus-7. It was followed by the Active Cavity Radiometer for Irradiance Monitoring (ACRIM) I on SMM (Willson et al., 1981), the Earth Radiation Budget Experiment (ERBE) on ERBS (Lee et al., 1995), ACRIM-II on UARS (Willson, 1994), Variability of Irradiance and Gravity Oscillations (VIRGO) on SoHO (Fröhlich et al., 1997), ACRIM-III on ACRIMSAT (Wilson, 2001) and the Total Solar Irradiance Monitor (TIM) on SORCE (Kopp and Lawrence, 2005).

The measurements disclosed that the value previously called the solar constant in fact varied at various time scales, from minutes to decades. The typical magnitude of variations in the last 3 cycles was about 0.1%, although changes up to about 0.3% were recorded on shorter time scales (days), e.g. around the Halloween storm at the end of October 2003.

Since none of the instruments survived over the whole period since 1978 and each of them suffers from its individual degradation, calibration or other problems, a construction of a composite TSI record is quite a challenge. Therefore, 3 different composites are now available: from the Physikalisch-Meteorologisches Observatorium Davos (PMOD; Fröhlich, 2006), the ACRIM

team (Willson and Mordvinov, 2003) and the Institut Royal Meteorologique Belgique (IRMB Dewitte et al., 2004).

They show certain differences, of which the most important regards the presence or absence of an upward secular trend between the minima preceding cycles 22 (1986) and 23 (1996). This long-standing argument traces its origin back to the unforeseen gap between the first two ACRIM experiments (July 1989 to October 1991), known as the ACRIM gap. Although 2 other experiments, HF and ERBE, continued operating during these 2 years, they are claimed to be lower precision experiments by Scafetta and Willson (2009). Moreover, the ERBE made measurements only approximately every second week, whereas in September 1989 the output signal of the HF radiometer saturated and the instrument was switched off for several days. Once back in operation, it showed an abrupt increase in irradiance by about  $0.4 \text{ W/m}^2$ . Somewhat later another increase of similar magnitude was reported (Lee et al., 1995; Chapman et al., 1996). Depending on whether this change is taken into account (as in the PMOD composite) or not (ACRIM), the composite time series shows either no change in the TSI average level from 1986 to 1996 (Fröhlich, 2006) or a significant increase (Willson and Mordvinov, 2003).

Another uncertainty of the TSI record regards the absolute level of the irradiance. The uncertainty in the absolute values of the TSI is significantly higher than that of the relative changes. In particular, there remains an unexplained difference of about  $4.5 \text{ W/m}^2$  between SORCE/TIM measurements and other currently operating instruments (Kopp et al., 2005). A comparison of the TIM measurements to the NIST (National Institute of Standards and Technology) reference detectors showed a rather good agreement thus

providing support to TIM's lower values. The future Glory mission of NASA promises to throw light on this, since the TSI measured with the Glory/TIM instrument will, for the first time, be compared directly to the TSI measurements by the reference cryogenic radiometer under the same vacuum conditions. For studies of climate change, variations in the TSI are of greater importance than the exact absolute value.

### *2.1.2. Spectral Irradiance*

The record of spectral irradiance measurements, accurate enough to assess its variations, goes back to the launch of the Solar Mesospheric Explorer (SME) in 1981. Although data between 115 and 302 nm were obtained, their accuracy is not sufficiently high due to degradation problems. This led to the introduction of the Mg II core-to-wing index, which, being a ratio of the fluxes measured at close-by wavelengths (Heath and Schlesinger, 1986; Viereck and Puga, 1999), suffers significantly less from instrument degradation. Mg II observations were continued by a number of following missions and a composite time series was produced by Viereck et al. (2004).

The Upper Atmosphere Research Satellite (UARS) launched in 1991 had 2 instruments for measurements of solar UV irradiance between approximately 115 and 420 nm, the Solar Ultraviolet Spectral Irradiance Monitor (SUSIM; Brueckner et al., 1993) and the Solar Stellar Comparison Experiment (SOLSTICE; Rottman et al., 1993). UARS SUSIM and SOLSTICE measurements revealed the strong spectral dependence of the solar irradiance variations (see, e.g., the review by Floyd et al., 2003). However, the variability above approximately 300 nm remained rather uncertain due to insufficient long-term stability of both instruments.

Since 1996 measurements have also been taken in three spectral channels centered at 402, 500 and 862 nm with the VIRGO Sun PhotoMeter (SPM) on SoHO (Fröhlich et al., 1997). The detectors are, however, not stable enough to allow an independent estimate of the comparatively weak longer-term trends at these wavelengths.

Data in a broader spectral range became available with the launch of the Solar Radiation and Climate Experiment (SORCE; Rottman, 2005) and the Environmental Satellite (ENVISAT) in 2003. SORCE has two instruments for measuring solar spectral irradiance: SOLSTICE and the Spectral Irradiance Monitor (SIM) operating at 115–425 nm and 200–2700 nm, respectively (Snow et al., 2005; Harder et al., 2005). The SCanning Imaging Absorption spectroMeter for Atmospheric CHartography (SCIAMACHY) on ENVISAT observes in the range 240–2380 nm (Skupin et al., 2005). The data from SIM and SCIAMACHY provided, for the first time, information about solar variability in the IR part of the spectrum and about longer-term (time scales of years) variations above 300 nm (Harder et al., 2009; Pagaran et al., 2009). These observations cover only the descending phase of solar cycle 23. The data over broad spectral sub-intervals are available, although there are still some remaining problems in some others (in particular, in the IR).

In 2008, the SOLar SPECTrum (SOLSPEC) instrument on SOLAR/ISS started observations between 165 nm and 3080 nm (Thuillier et al., 2009). The data are not yet publicly available.

Note that here we only discuss the spectral range above 115 nm. Variations of the irradiance at yet shorter wavelengths is of more interest for space weather studies and their measurements and modelling have recently been

reviewed by Woods (2008).

## *2.2. Sources of irradiance variations*

Just a view of the solar surface with a modern telescope (and to some extent even without) suggests that brightness of the solar disc is not homogeneous and changes in time. Sunspots are the largest magnetic structures on the solar surface and have been seen already in antiquity with the naked eye. Being cooler than the surrounding photosphere, they appear darker. Thus a passage of a spot across the visible solar disc causes a dip in solar brightness (see, e.g., Hudson et al., 1982; Fligge et al., 2000). The spots appear particularly dark when they are close to the disc centre when their projected area is largest and the dark umbra is best visible. The related irradiance changes occur on time scales of hours to about 10 days.

Since the amount of and area covered by sunspots increases significantly from activity minimum to cycle maximum, the frequency and depths of brightness dips related to spots also increase considerably. Some of the dips reach up to  $3\text{--}4\text{ W/m}^2$  (or about 0.2–0.3%). On average, however, the Sun brightens from cycle minima to maxima. This is because of the contribution of faculae and the network, which are weaker magnetic elements appearing bright on the solar surface (Zwaan, 1978; Solanki, 1993). Faculae are formed in active regions and typically appear in the vicinity of sunspots. The weaker network elements are spread over the whole disc, forming a bright network at the intersections of supergranules. In the visible continuum, the contrast of faculae is significantly higher close to the limb. Thus when a facular region crosses the visible solar disc it typically causes a weakly double-peaked brightening (see, e.g., Fligge et al., 2000).



Wenzler (2005) has considered the net contributions of sunspots and faculae to the TSI variation of cycle 23. He found that sunspots caused a darkening of about  $0.84 \text{ W/m}^2$ , whereas faculae produced a brightening of about  $1.73 \text{ W/m}^2$ . The net increase in the TSI thus was  $0.89 \text{ W/m}^2$  in good agreement with the value of  $0.829 \pm 0.017 \text{ W/m}^2$  given by the PMOD composite (Fröhlich, 2006).

Variations in the brightness of the Sun are also produced by the continuously evolving granulation pattern. Granules are signatures of convective cells with sizes ranging from a few hundred to roughly 2000 km. Their central parts, where hot material streams up from the interior to the surface, appear brighter, whereas at the outer edges the cooled darker material flows down, producing an RMS contrast of approximately 14% in the green part of the solar spectrum (Danilović et al., 2008). The typical lifetimes of granules are about 5 to 10 minutes (Hirzberger et al., 1999). Granulation dominates irradiance variations on time scales shorter than approximately half a day and is not important for the Earth’s climate (Solanki et al., 2003).

### *2.3. The fundamentals of the SATIRE model*

Here we describe the basic assumptions and ingredients of SATIRE, a set of codes to calculate spectral solar irradiance from solar disc images or activity proxies such as sunspot numbers (Fligge et al., 1998; Krivova et al., 2003, 2007; Wenzler et al., 2006). The assumption underlying SATIRE is that all changes in the solar irradiance on time scales longer than hours are solely due to changes in the solar surface magnetic flux as traced through surface features, such as spots and faculae (see Sec. 2.2 for more detail). To obtain the solar irradiance at a given time,  $t$ , and wavelength,  $\lambda$ , it then

suffices to derive filling factors,  $f^a(t)$ , quantifying how much of the solar surface is covered by a given surface feature  $a$  (where  $a$  denotes umbra, penumbra, faculae or network), and to calculate the emergent radiative flux of the feature  $F^a(\lambda)$ . The solar irradiance,  $S(t, \lambda)$ , can then be calculated by summing the emergent radiative fluxes of the quiet (inactive) Sun,  $F^q(\lambda)$ , and those of the surface features according to filling factors

$$S(t, \lambda) = \sum_a f^a(t) F^a(\lambda) + \left(1 - \sum_a f^a(t)\right) F^q(\lambda). \quad (1)$$

This formalism can be extended to include positional information, in which case the global filling factors  $f^a$  are replaced by local filling factors  $\alpha_{i,j}^a$ , where  $i, j$  are indices referring to a particular pixel in a solar image or magnetogram. The radiative fluxes  $F^a$  are replaced by intensities  $I^a(\mu)$ , where  $\mu = \cos \Theta$  and  $\Theta$  is the heliocentric angle. Then Eq. (1) needs to be replaced by

$$S(t, \lambda) = \sum_a \sum_{i,j} \left[ \alpha_{\mu(i,j)}^a(t) I_{\mu(i,j)}^a(\lambda) + (1 - \alpha_{\mu(i,j)}^a(t)) I_{\mu(i,j)}^q(\lambda) \right]. \quad (2)$$

Note that the radiative fluxes are independent of time; their calculation is discussed in the following paragraphs. The filling factors represent the changing aspect of the solar surface, and it is their time dependence that produces the variability in the solar irradiance. The filling factors can be obtained from a variety of data sets, depending on the time scales considered. The type of data available also determines whether Eq. (2) is employed (basically limited to the satellite era) or Eq. (1), for the longer time scales. In order to distinguish between models adjusted to different time scales and based on different kinds of input data used to derive the filling factors, we call

them SATIRE-S (Satellite period, magnetogram-based, Sect. 3), SATIRE-T (Telescope era, from the sunspot number, Sect. 4) and SATIRE-M (Millennia time scales, based on cosmogenic isotope data, Sect. 5). Note, that positional information for the photospheric magnetic features is only available in case of SATIRE-S, when magnetograms are used to derive the filling factors.

The emergent intensities are calculated from a set of model atmospheres using ATLAS9 (Kurucz, 1993, 2005). This yields relatively low-resolution spectra (1 to 2 nm in the NUV and optical), but has the advantage of covering the whole wavelength range contributing significantly to the TSI while remaining computationally manageable. As ATLAS9 uses an LTE approach and combines the opacity contributions due to lines into opacity distribution functions, the accuracy of the calculations decreases at shorter wavelength and for the strongest lines. For these wavelength regions, more reliable results can be obtained using a correlation analysis as described in Krivova et al. (2006).

The model atmospheres and resulting emergent intensities are described in detail by Unruh et al. (1999). The model for the quiet Sun is based on the standard solar model of Kurucz (1992); the umbral and penumbral models are radiative equilibrium atmosphere models with effective temperatures of 4500 K and 5400 K, respectively. The facular model, finally, is a modified version of FAL P from Fontenla et al. (1993).

Solar irradiance reconstructions based on these models have been used successfully to calculate the spectral variability over a large range of wavelengths (see Sec. 3.3); they also match the measured TSI on solar-cycle timescales (Sec. 3.2). Despite these successes, a number of issues remain.

One of these is that the use of 1-D atmospheres leads to the facular contrast being overestimated towards the solar limb. Another is the assumption that all small-scale magnetic features are assumed to display the same wavelength and limb-dependent contrast behaviour that is scaled according to their magnetic flux. This assumption is unlikely to hold, as suggested by the different thermal structure of network and active region flux tubes (Solanki, 1986) and the magnetic flux dependence of facular/network contrast (Topka et al., 1997; Ortiz et al., 2002). One way to address both of these issues is to use realistic simulations of magneto-convection in order to represent the 3-D structure of the solar atmosphere and to derive from them the emergent intensities as a function of the magnetic flux.

The first steps of such an approach were presented by Unruh et al. (2009), who used MURaM magneto-convection simulations (Vögler et al., 2005) to calculate disc-centre intensities. Figure 1 shows first results for contrasts at  $\mu = 1$  (i.e. solar disc centre) derived from magneto-convection simulations with mean magnetic fluxes of 50 G, 200 G and 400 G. Also shown is the contrast currently used in the SATIRE reconstructions (dotted line); it has been reduced by approximately 30% so that it can be compared directly to the simulation results. A higher contrast is expected for the SATIRE 1-D model as this represents the brightest faculae, while the MURaM contrast is averaged over a computational box that contains a mix of magnetic flux tubes and field-free regions.

Overall, the spectral behaviour of the 200-G simulations and of the SATIRE contrasts is very similar. The 50-G simulations that are more indicative of the solar network show a slightly flatter spectral shape with a slower increase

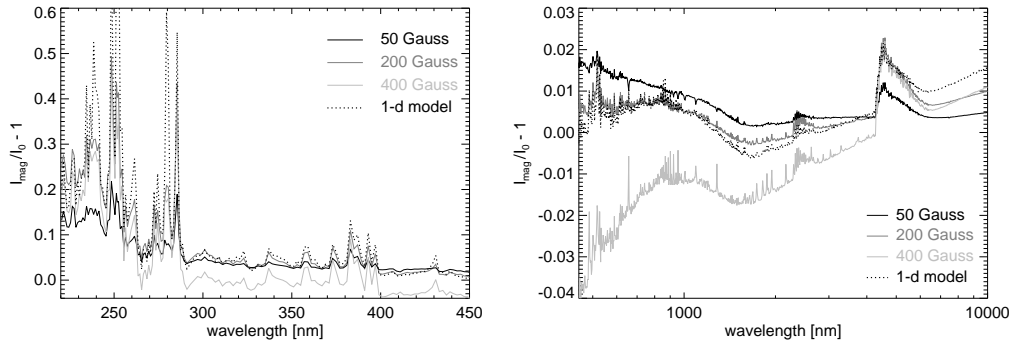


Figure 1: Disk-centre contrasts of simulated convection with a mean magnetic flux of 50 G, 200 G and 400 G compared to a non-magnetic model. The dotted line shows the contrast of the 1-D facular atmosphere used in the SATIRE reconstructions. This has been reduced by 30% for ease of comparison.

of the contrast at shorter wavelengths and less darkening in the near-infrared.

### 3. Solar Irradiance Over the Satellite Period (SATIRE-S)

#### 3.1. Temporal Changes from Magnetograms

The most detailed information on the temporal evolution of the solar surface magnetic features, needed in order to calculate irradiance variations, is provided by full disc magnetograms. Since 1996 such magnetograms have been regularly recorded by the Michelson Doppler Imager (MDI) on SoHO (Scherrer et al., 1995). Ground-based magnetograms with a sufficiently large spatial resolution, e.g., from the Kitt Peak National Solar Observatory (NSO KP) are available back to 1974 (Livingston et al., 1976; Jones et al., 1992), although the temporal coverage and the quality become significantly poorer for the earlier period.

Magnetograms and continuum images recorded as close in time as possible are used to identify different magnetic features on the solar surface: sunspot umbrae, sunspot penumbrae, faculae and the network, and to determine which fraction of the solar surface is occupied by each component at a given  $\mu$ , i.e. the filling factors  $\alpha$  (see Sect. 2.3). Spot umbrae and penumbrae are identified by their continuum contrasts. Pixels belonging to spots are then excluded from the (co-aligned) magnetograms and the remaining magnetogram signal is considered to be faculae and the network. Pixels with the magnetic signal below the noise threshold are counted as quiet Sun.

The intensity spectra of all components are then weighted by the corresponding filling factors and summed up to give the irradiance as a function of wavelength using Eq. (2). Integration over all wavelengths results in total solar irradiance at time  $t$ . The procedure is repeated for every day when a magnetogram and a continuum image are available. The models employing MDI and NSO KP data are described in detail by Krivova et al. (2003) and Wenzler et al. (2004, 2005, 2006), respectively. Wenzler et al. (2004) also compared the reconstructions based on these 2 sets of magnetograms to each other.

The model has a single free parameter,  $B_{\text{sat}}$ , the value of the magnetogram signal at which magnetic field in the solar photosphere fills the whole magnetogram pixel  $(i, j)$ .  $B_{\text{sat}}$  is found from the best agreement with the TSI measurements. Note that one aim of the recently started work on computing the spectra from MHD simulations (see Sect. 2.3) is to do away with this free parameter.

### 3.2. Total Solar Irradiance

Krivova et al. (2003) employed MDI magnetograms to reconstruct the TSI between 1996 and 2002. Excellent agreement between the PMOD TSI composite and the model was obtained with a correlation coefficient of  $r_c = 0.96$  ( $r_c^2 = 0.92$ ). Wenzler et al. (2004, 2005, 2006) have extended this reconstruction back to 1974 using NSO KP magnetograms and continuum images. The correlation for the whole period 1974–2003 is somewhat lower than when MDI data are used ( $r_c = 0.91$ ,  $r_c^2 = 0.83$ ), which is not surprising due to the significantly lower quality and artefacts seen in ground-based data (especially before 1992 when an older instrument was used at the NSO KP) compared to those taken from space. Nevertheless, the good agreement between the data and the model provides strong support for the model’s basic assumption, namely that the dominant part of the irradiance variations on time scales longer than about a day is caused by the evolution of solar surface magnetic features.

Wenzler et al. (2009) have also compared the model to all three currently available TSI composites: PMOD, ACRIM and IRMB. For this, they have varied the value of the single free parameter ( $B_{\text{sat}}$ , see Sect. 3.1) in order to find the best fit to each of the composites individually. The overall best fit is found with the PMOD composite ( $r_c = 0.91$ , slope 0.98), whereas the agreement with the other two composites is markedly poorer ( $r_c = 0.79$ , slope 0.82 for ACRIM and  $r_c = 0.82$ , slope 0.81 for IRMB). This can be judged from Fig. 2, which displays the difference between the TSI reconstructed by SATIRE-S and each of the three composites.

Scafetta and Willson (2009) proposed that these reconstructions can be

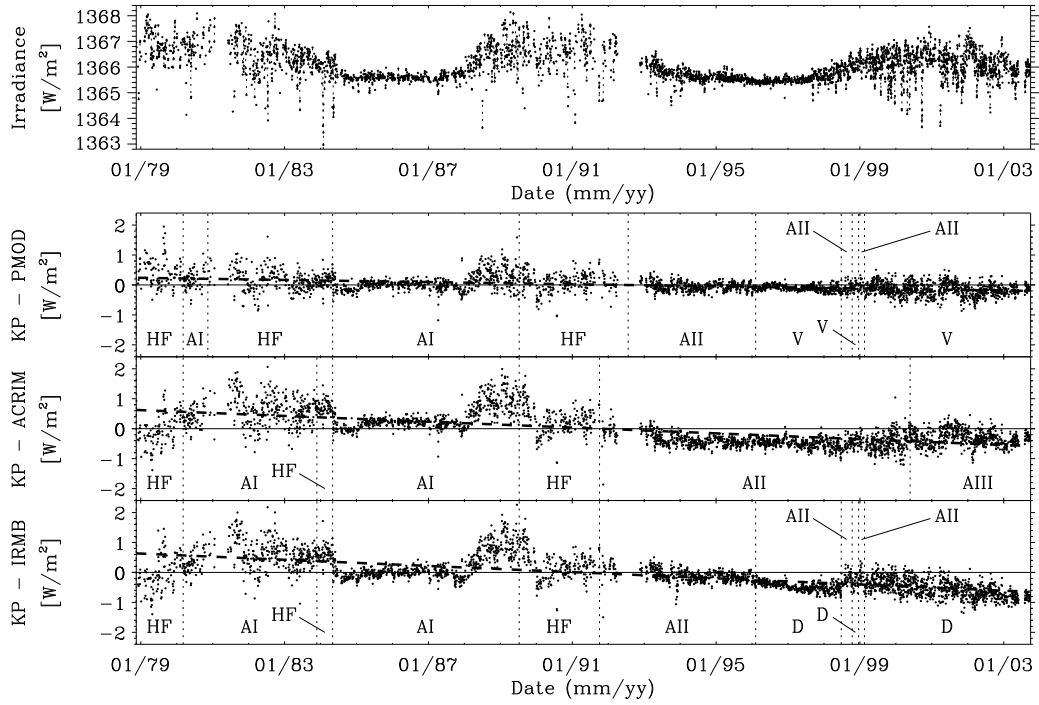


Figure 2: The *top panel* shows the reconstructed daily total solar irradiance based on NSO KP data for 3528 days between 1978 and 2003, i.e. from the late rising phase of cycle 21 to the declining phase of cycle 23. The three *lower panels* show the difference between the reconstructed TSI and the PMOD, ACRIM and IRMB composites, respectively. Each dot represents a daily value. The horizontal solid lines indicate a difference = 0, the thick dashed lines are linear regressions. The dotted vertical lines indicate periods when the individual data sets from HF, AI, AII & AIII (ACRIM I, II & III), V (VIRGO: Variability of solar IRradiance and Gravity Oscillations experiment on SoHO) and D (DIARAD: Differential Absolute RADiometer) were used for the composites. From Wenzler et al. (2009)



used to bridge the so-called ACRIM gap (see Sect. 2.1.1) and to create a ‘mixed’ ACRIM-1 – SATIRE – ACRIM-2 composite. They have compared ACRIM-1 and ACRIM-2 data directly to the model, in order to cross-calibrate the data from the two instruments. These authors have, however, used the SATIRE-T model described in Sect. 4, which is not suited for such an analysis. As discussed later, SATIRE-T is based on the historic sunspot number record instead of on magnetograms and continuum images, so that it is based on Eq. (1) rather than the more realistic Eq. (2). It is therefore significantly less accurate than SATIRE-S on time scales of weeks to several months. These are, however, the most critical time scales for such a comparison of the data and the model. This indicates that caution needs to be exercised when considering the results of Scafetta and Willson (2009), in particular their conclusion about the upward trend between the minima in 1986 and 1996.

Krivova et al. (2009a) have repeated this analysis employing the more appropriate SATIRE-S model. The ‘mixed’ ACRIM-1 – SATIRE-S – ACRIM-2 composite is shown in Fig. 3. It shows no increase in the TSI from 1986 to 1996, in contrast to the ACRIM composite. Actually, a slight decrease is found. The magnitude of this decrease cannot be estimated very accurately from such an analysis but it lies between approximately 0.2 and 0.7 W/m<sup>2</sup> (0.013–0.05%).

### *3.3. Spectral Solar Irradiance*

Early comparisons between SATIRE-S spectral irradiance reconstructions and UARS/SUSIM measurements were presented by Krivova and Solanki (2005) and Krivova et al. (2006) for wavelengths below 400 nm. These com-

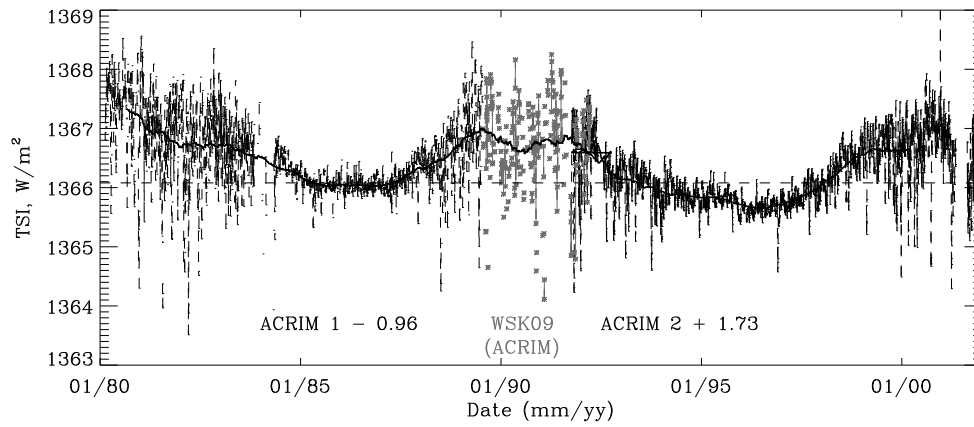


Figure 3: 'Mixed' TSI composite constructed from ACRIM-1 and ACRIM-2 data (black dashed line), with the gap bridged using the SATIRE-S (WSK09 ACRIM) model (asterisks connected by grey solid line when there are no gaps). The heavy solid line is the 1-year smoothed TSI, and the horizontal dashed line shows the level of the minimum preceding cycle 22. From Krivova et al. (2009a).

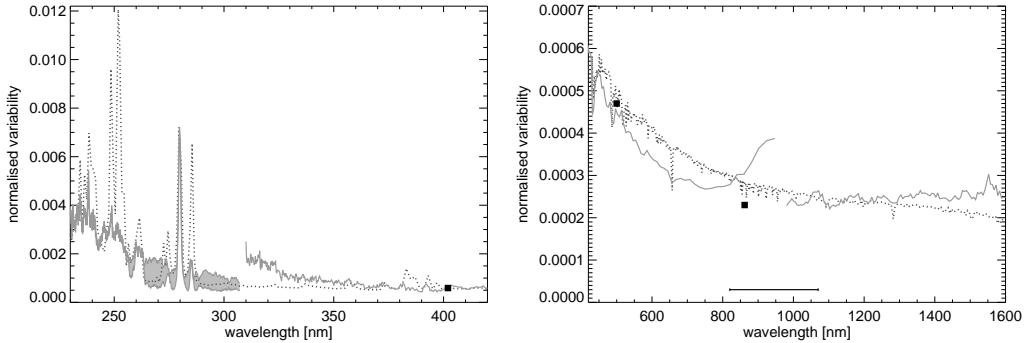


Figure 4: Normalised variability from May 2004 to July 2004 as measured with *SORCE/SIM* (solid lines) and modelled with *SATIRE* (dotted lines) for wavelengths spanning 230 nm to 420 nm (left-hand side) and 420 nm to 1600 nm (right-hand side). The filled squares indicate the variability measured in the three *SoHO/VIRGO* SPM bands at 402 nm, 501 nm and 863 nm.

comparisons showed that there is good agreement between the measured and modelled wavelength integrated flux between 220 and 240 nm.

Krivova et al. (2006) then used this wavelength band as a reference to derive regression coefficients measuring the response of those wavelength regions that are not well represented by the *ATLAS9* fluxes. In this way *SATIRE* can be extended down to 115 nm. For wavelengths above 270 nm, the sensitivity of *UARS/SUSIM* is not sufficient to measure solar variability reliably, so that modelled fluxes (i.e. those based on model atmospheres) are currently more reliable.

Comparisons in the visible and near-infrared have only become possible with the launch of *SORCE* and *ENVISAT* (Sect. 2.1.2). First results from *SORCE/SIM* were presented by Fontenla et al. (2004). Comparisons between *SIM* data and *SATIRE-S* covering 3 solar rotations in 2004 were

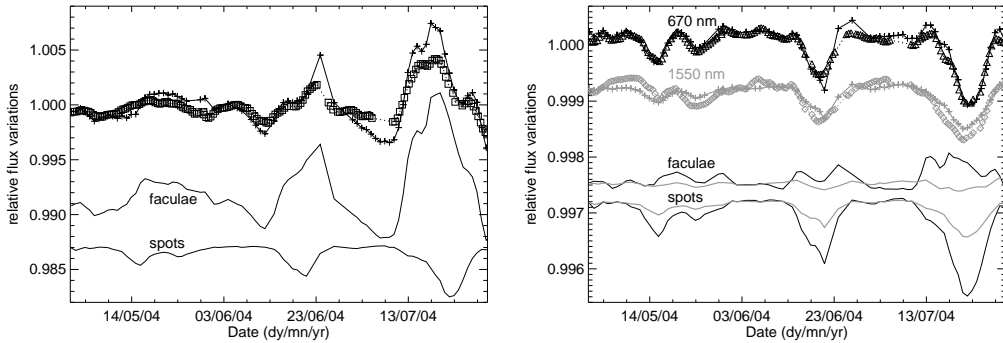


Figure 5: *Top curves:* flux variations for the Mg II band (*left-hand side*) and for two bands centred at 670 and at 1550 nm (*right-hand panels*). The dotted lines linking the squares and triangles represent SIM data, the plus signs linked by the solid lines show the model calculations. *Bottom curves:* modelled times series for the facular and spot contributions. The upper lines are for the faculae, the lower for the spots. Following Unruh et al. (2008).

carried out by Unruh et al. (2008). The measured and modelled variability is shown in Fig. 4. There is good agreement between SATIRE-S and SORCE/SIM, in particular for wavelengths above 360 nm. Between 310 nm and 360 nm detailed comparisons are hampered as the sensitivity of the detector is not quite sufficient to measure solar variability adequately and the modelled irradiances yield more reliable results. For wavelengths above 550 nm SATIRE-S shows a slightly flatter decrease in variability than the SORCE measurements, though detailed light-curve comparisons show excellent agreement in the short-term variability.

Figure 5 shows measured and modelled time series for the Mg II band (left-hand side) and for two bands centred at 670 and at 1550 nm, respectively (right-hand panels). The upper curves in the plots show the measured and modelled solar variability while the bottom curves show the modelled

contributions of the faculae and spots to the irradiance variations. The figures illustrate the change in the lightcurve aspects as one moves from the UV to the near-IR. In the UV, as illustrated by the Mg II (at around 280 nm) band, the influence of the spots is so small that their darkening effect is more than compensated for by the faculae, even on solar rotational time scales. Furthermore, the facular contrast increase towards the limb is not sufficient to counteract the projection effects and the Sun appears brightest when the spot groups are at disc centre. At longer wavelengths (e.g., at 670 nm), the facular brightenings are much weaker and show a double-peaked structure. Thus faculae produce most of the brightening when near the limb and very little, if any, when at disc centre. In the near-IR (as illustrated by the 1550 nm band), only very little facular brightening is seen close to the limb, which is compensated by the earlier onset and longer duration of spot darkening. The overall effect of faculae at 1550 nm is one of darkening.

Krivova et al. (2009b) have reconstructed solar UV irradiance in the range 115–400 nm over the period 1974–2007 by making use of the empirical extension of the SATIRE models by Krivova et al. (2006) employing SUSIM data. The evolution of the solar photospheric magnetic flux in this case was described by the magnetograms from the KP NSO between 1974 and 2003 and by the MDI instrument on SoHO since 1996. The gaps in daily data were filled using the Mg II core-to-wing ratio and the solar F10.7 cm radio flux.

Figure 6 shows the reconstructed solar Ly- $\alpha$  irradiance (light grey crosses; red in online version), SUSIM measurements (grey dashed line / green) and the composite time series (black dotted line / blue) compiled by Woods et al.

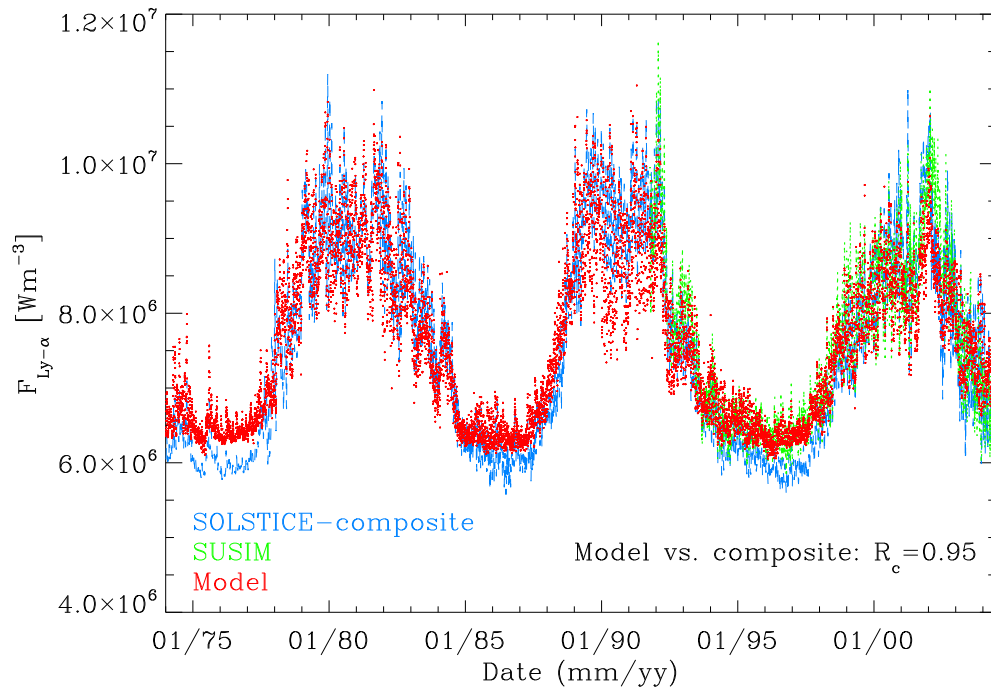


Figure 6: Solar Ly- $\alpha$  irradiance since 1974: reconstructed by SATIRE-S (light grey crosses; in online version red), measured by the SUSIM instrument (grey dashed line; in online version green) and compiled by Woods et al. (2000; black dotted line; in online version blue). From Krivova et al. (2009).

(2000). The latter record includes measurements from the Atmospheric Explorer E (AE-E, 1977–1980), the Solar Mesosphere Explorer (SME, 1981–1989), UARS SOLSTICE (1991–2001) and the Solar EUV Experiment (SEE) on the TIMED mission launched in 2001. The gaps are filled in using proxy models based on Mg II and F10.7 indices. The F10.7-based model is also used for the period before 1977. All measurements and models are adjusted to the SOLSTICE absolute values. The model agrees well with the SUSIM data, which confirms that the semi-empirical technique works well. There is some difference in the magnitude of the Ly- $\alpha$  solar cycle variation between SOLSTICE and SUSIM, which remains also if the model is compared to the composite. This is because the model is adjusted to SUSIM by construction. Other than that the model agrees with the composite record very well with a correlation coefficient of 0.95.

Employing the solar F10.7 cm radio flux data (Tanaka et al., 1973), it is possible to extend the reconstruction back to 1947. For this, the radio flux measurements are used to calculate the irradiance at 220–240 nm, in the same way as done by Krivova et al. (2009b), who employed these data in order to fill in the gaps in their reconstructions for the period 1974–2007. Irradiance at other wavelengths is then calculated from the irradiance in the reference range, 220–240 nm, by applying the technique of Krivova et al. (2006) described above. Figure 7 shows the reconstructed solar irradiance integrated over spectral ranges of particular interest for climate studies as a function of time: (a) 130–175 nm, (b) 175–200 nm, (c) 200–242 nm, (d) 200–350 nm, (e) 800–1500 nm and (f) 1500–2500 nm. The model is based on radio flux data before 1974 and on magnetograms after 1974. Solar UV irradiance

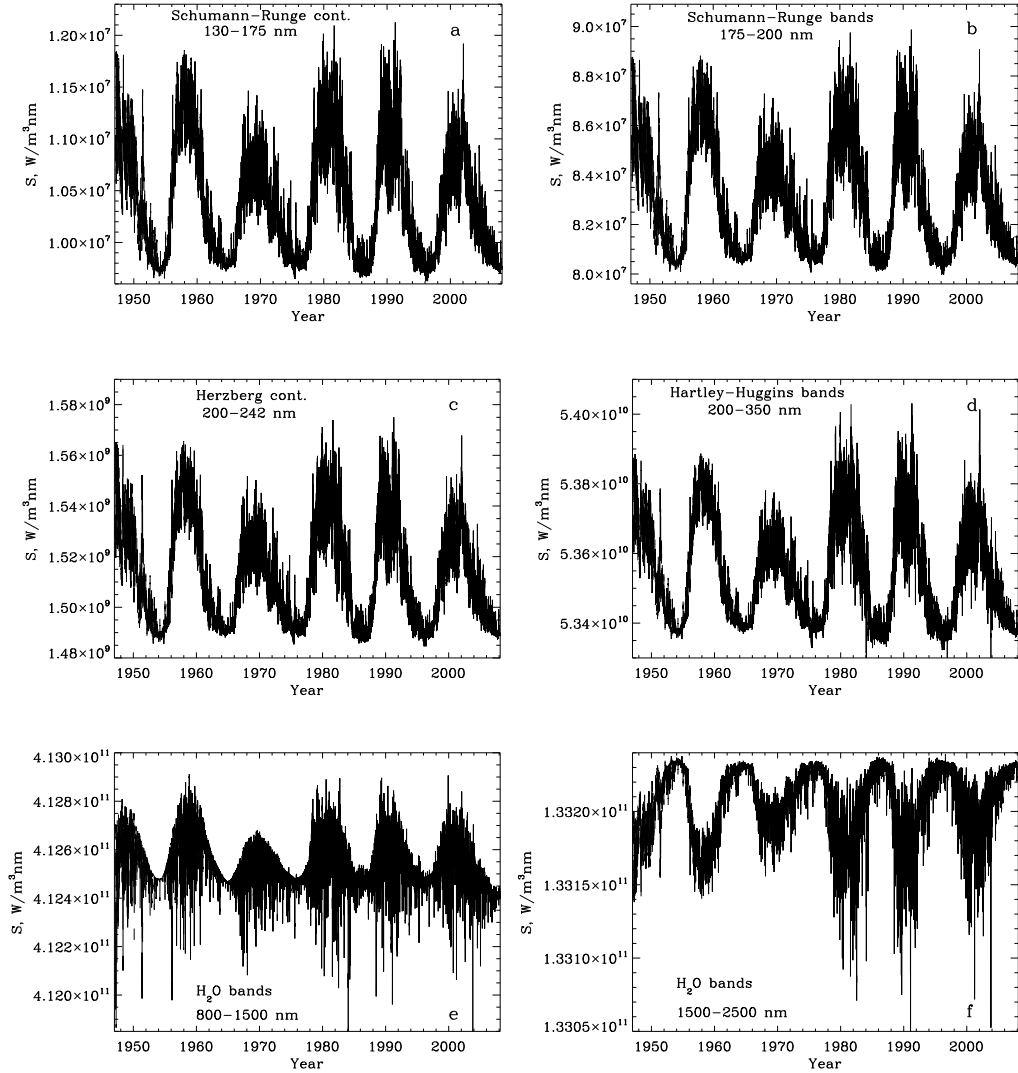


Figure 7: Reconstructed solar irradiance in the period 1947–2007 integrated over the wavelength ranges: (a) 130–175 nm (Schumann-Runge continuum), (b) 175–200 nm (Schumann-Runge bands), (c) 200–242 nm (Herzberg continuum), (d) 200–350 nm (Hartley-Huggins bands), (e) 800–1500 nm ( $\text{H}_2\text{O}$  bands) and (f) 1500–2500 nm ( $\text{H}_2\text{O}$  bands).



(panels a–d) varied by a factor 10 to 100 more than the TSI. Interestingly, the irradiance in the range between around 1500 nm and 2500 nm (panel f) shows an inverse solar cycle variation compared to the TSI and other spectral ranges. This inverse variation was also noticed by Harder et al. (2009) from the analysis of SORCE data. This is due to the low or even negative contrast of faculae at these wavelengths (Unruh et al., 2008, see also Fig. 5), so that their brightening (if any) no longer compensates darkening due to sunspots.

#### **4. Solar Irradiance Since the Maunder Minimum (SATIRE-T)**

##### *4.1. Temporal Changes from the Sunspot Number*

The advantage offered by high resolution magnetograms of having information on the spatial distribution of the solar surface magnetic features as well as the magnetic field strength is not available prior to 1974. Models going further back in time have to content themselves with sparser data. One such historic record is the sunspot number. It is widely used for reconstructions of solar irradiance on time scales longer than a few decades and is, in fact, the only direct proxy of solar magnetic activity going back to the Maunder minimum (a period of unusually low solar activity in the 17th century).

Solanki et al. (2000, 2002) have constructed a physical model which allows a reconstruction of the evolution of the solar photospheric magnetic field from the sunspot number. In this way, it is possible to calculate not just the total magnetic flux emerging on the solar surface at a given time, but also individual contributions of different components: active regions (sunspots and faculae), ephemeral regions (smaller short-lived bipolar magnetic regions) and the open flux (a small part of the photospheric magnetic flux whose

field lines reach into the heliosphere). The calculated open magnetic flux is found to be in good agreement with the empirical reconstruction of the heliospheric magnetic field since 1868 by Lockwood et al. (1999, 2009) from the geomagnetic *aa*-index. Also, the modelled total photospheric magnetic field reproduces the measurements since 1974 carried out at the Mt. Wilson, Kitt Peak and Wilcox Solar Observatories (Arge et al., 2002; Wenzler et al., 2006).

Krivova et al. (2007) and Balmaceda et al. (2007) made use of this model in order to also reconstruct solar total irradiance since 1700 and 1610, respectively. In order to calculate the filling factors (Sect. 2.3) of sunspots as a function of time, they employed the sunspot areas. These have been measured since 1874 (see Balmaceda et al., 2009) and were derived for the earlier period using a linear relationship between sunspot areas and numbers. The sunspot contribution is then subtracted from the active region magnetic flux to assess the flux present in the form of faculae. The sum of the ephemeral region and open magnetic flux describes the evolution of the network.

The network and facular magnetic fluxes are then converted into corresponding filling factors (see Sect. 2.3) assuming that the filling factors are proportional to the corresponding magnetic field strengths until the saturation limit ( $B_{sat}$ , Sect. 3.1) is reached. Finally, the irradiance is calculated by summing up disc-integrated brightnesses (i.e. radiative fluxes) of different components (the quiet Sun, sunspot umbrae, sunspot penumbrae, faculae and the network) weighted by their filling factors as described in Sect. 2.3. In addition to the heliospheric flux reconstruction by Lockwood et al. (1999) and the total magnetic flux data, the model also reproduces well the mea-

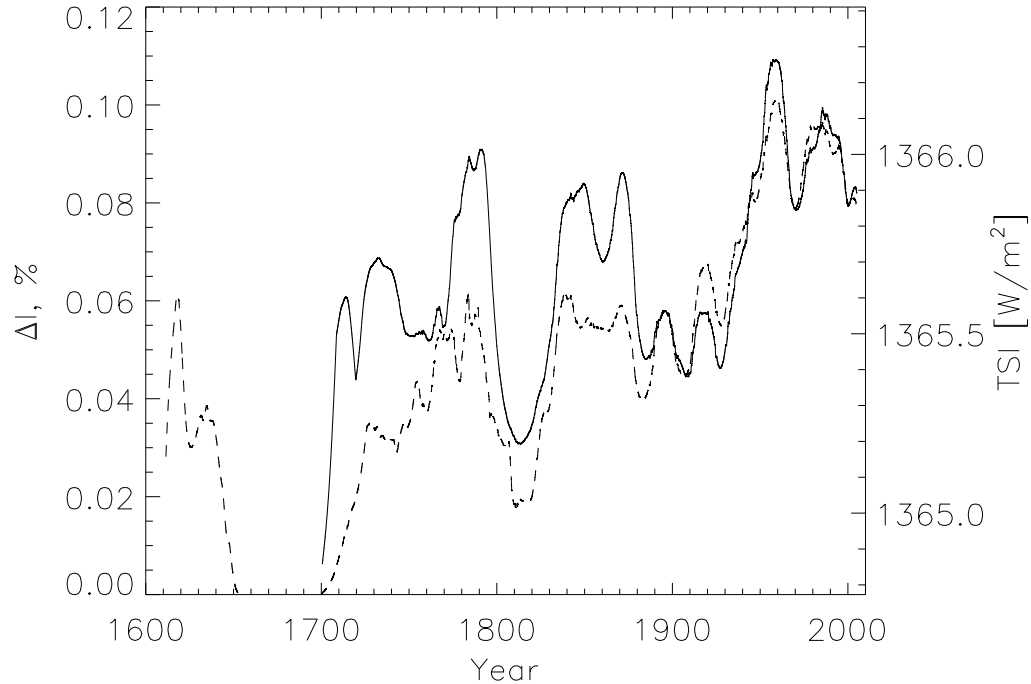


Figure 8: 11-yr running mean of the reconstructed TSI based on the Zurich (solid line) and Group sunspot number (dashed line).

sured TSI since 1978, although the accuracy of the model is reduced on time scales of weeks to about a year (Krivova et al., 2009a, see Sect. 3.2).

#### 4.2. Irradiance

Krivova et al. (2007) have employed the Zurich sunspot number in order to reconstruct solar total irradiance since 1700, whereas Balmaceda et al. (2007) used the Group sunspot number in order to go back to 1610. The two reconstructions are shown in Fig. 8. They show slightly different irradiance levels during the 18th and 19th centuries, but both suggest that, averaged over 11 years, the TSI has increased by about  $1.3 \text{ Wm}^{-2}$  since the end of

the Maunder minimum. By applying different assumptions regarding the evolution of the ephemeral region magnetic flux, Krivova et al. (2007) have also estimated the uncertainty range as 0.9 to 1.5  $\text{Wm}^{-2}$ . The lower limit is in good agreement with the results of the modelling effort by Wang et al. (2005), who neglected the extended length of the ephemeral region cycle, which is the main source of the secular trend in the SATIRE-T model. The upper limit of 1.5  $\text{Wm}^{-2}$  is close to the value of 1.7  $\text{Wm}^{-2}$  from Foster (2004), cf. Lockwood (2005), who assumed that the network disappeared completely during the Maunder minimum. A comparably low value for the magnitude of the secular increase has also been obtained by Crouch et al. (2008) from their model of TSI variations. The model does not, however, go back to the Maunder minimum, but stops at 1874.

All recent estimates of the magnitude of the secular trend are thus significantly lower than the values deduced earlier from stellar data (Baliunas and Jastrow, 1990; White et al., 1992; Lean et al., 1995). Nevertheless, even though all recent models agree that TSI increased by significantly less than 2  $\text{Wm}^{-2}$  since the Maunder minimum, considerable uncertainty remains. This is because all models have free parameters, or make assumptions that cannot be rigorously tested.

A potential independent source of information on the magnitude of the secular trend are the historic archives of full-disc solar images in the Ca II K line. Such observations were carried out by a number of observatories around the globe since the beginning of the 20th century. Some of the archives have recently been digitised. Earlier analysis of the digitised data was presented by, e.g., Kariyappa and Pap (1996); Foukal (1996); Caccin et al. (1998); Worden et al.

(1998). Usage of these data is until now limited because of the numerous problems and artifacts affecting the images, such as plate defects and aging, degradation of instrumentation and observing programmes, geometrical distortions, photometrical uncertainties etc. (Ermolli et al., 2007). Ermolli et al. (2009) have analysed the quality of the data of 3 digitised historic archives from Arcetri, Mt. Wilson and Kodaikanal observatories. They have also been able to fix some of the problems, such as, e.g., disc eccentricity. Some others are more difficult to correct. These include photometric uncertainties (due to, e.g., stray light or missing photographic calibration) and changes in the image content with time (due to, e.g., varying wavelength of the observations).

Ermolli et al. (2009) have developed a method of image calibration independent of the calibration exposures and calculated plage coverage as a function of time for the 3 analysed archives (Fig. 9). The Pearson correlation coefficients for each pair of the data sets lie between 0.85 and 0.93. The most significant differences are found for cycles 15, 17 and 19, which are partly explained by the stray-light degradations at the beginning of each observing programme and by differences in the wavelength of observations. Similar results were obtained by Tlatov et al. (2009), who also analysed and compared Kodaikanal and Mt. Wilson observations (see their Fig. 4). These results suggest that caution is needed when using such data without careful analysis of their problems and intrinsic instrumental variations.

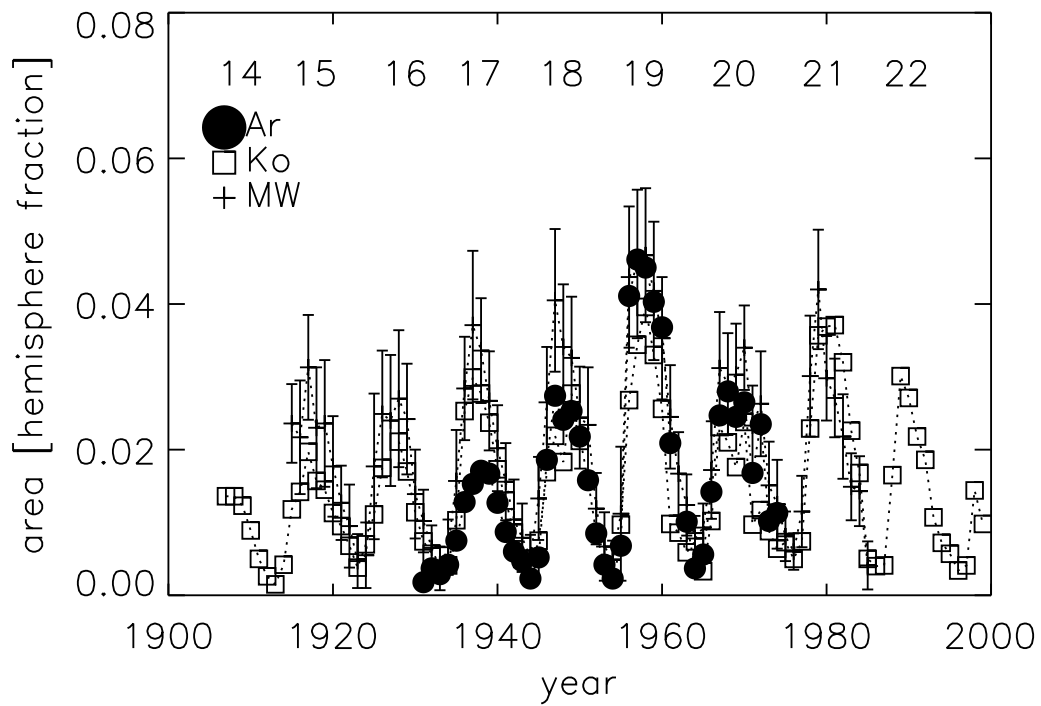


Figure 9: Temporal variation of yearly median values of the plage coverage measured from the Arcetri, Kodaikanal, and Mt. Wilson series. The error bars represent the standard deviation of measured values over the annual interval; for clarity, they are only shown for the MW series. Cycle numbers are given at the top of each cycle. From Ermolli et al. (2009)

## 5. Solar Activity Over the Holocene

Before 1610, no direct proxies of solar magnetic activity are available. The indirect proxies at hand are the concentrations of the cosmogenic isotopes  $^{10}\text{Be}$  and  $^{14}\text{C}$  in natural terrestrial archives. These isotopes are produced when high-energy cosmic rays enter the Earth's atmosphere and react with nitrogen and other atoms. The flux of the cosmic rays at the Earth is modulated by the solar open magnetic field, which makes it possible to reconstruct the open magnetic flux using the production rates of the cosmogenic radioisotopes.

Solanki et al. (2004) and Usoskin et al. (2004, 2006) have combined physics-based models for each of the processes connecting  $^{14}\text{C}$  and  $^{10}\text{Be}$  concentration with sunspot number and thus were able to reconstruct the sunspot number over the whole Holocene. This reconstruction has shown that the Sun is currently in a state of unusually high magnetic activity and that prolonged periods of very low solar activity similar to the Maunder minimum (grand minima) have regularly occurred in the past (see also Schove, 1955; Siscoe, 1980; Krivsky, 1984). Also periods of higher averaged solar activity, similar to the recent one (grand maxima) have occurred. Usoskin et al. (2007) give a list of all grand minima and maxima since 9500 BC detected in the reconstructed sunspot number record.

The reconstruction of solar irradiance for the Holocene is complicated by the fact that only a cycle-averaged sunspot number can be derived from the  $^{14}\text{C}$  and  $^{10}\text{Be}$  concentrations. Thus the SATIRE-T model described in Sect. 4 cannot be applied directly. Therefore, first relationships are derived, using the SATIRE-T results, between the cycle averaged open magnetic flux

(the primary solar quantity obtained from  $^{14}\text{C}$  and  $^{10}\text{Be}$  concentrations) and the total magnetic flux, the sunspot number and solar irradiance. These relationships are then used to calculate the solar irradiance over the Holocene (Vieira et al., in prep.).

## 6. Summary

As weak as they are (about 0.1% over the solar cycle), solar irradiance variations affect the Earth's climate at a level of 0.2°K over the solar cycle (Camp and Tung, 2007). The role of the total solar irradiance might be significantly reinforced by the wavelength dependence of irradiance variations. The amplitude of the variations is 1 to 3 orders of magnitude higher in the UV part of the spectrum than in the visible or IR. At the same time, solar UV radiation is an important driver of chemical and physical processes in the Earth's upper atmosphere.

Reliable assessment of solar forcing on the Earth's climate is still plagued, among other factors, by a shortage of reliable and sufficiently long irradiance records. The time series of direct space-borne measurements of solar irradiance is only 3 decades long (in case of spectral irradiance, even shorter). Therefore we have recently focussed our main attention on tests of the reconstructed irradiance against the newest spectral data, improvement of the models in the UV and appraisal of the magnitude of the secular trend in irradiance.

We have reconstructed solar spectral irradiance at 115–160000 nm back to 1947. Reconstruction of solar total irradiance goes back to 1610 and suggests a value of about 1–1.5  $\text{Wm}^{-2}$  for an increase in the cycle-averaged



TSI between the end of the Maunder minimum and the last 50 years, which is significantly lower than previously accepted but agrees with other recent estimates. First steps have also been made towards reconstructions of solar total and spectral irradiance on time scales of millennia.

**Acknowledgments.** This work was supported by the Deutsche Forschungsgemeinschaft, DFG project number SO 711/2 and by the WCU grant No. R31-10016 funded by the Korean Ministry of Education, Science and Technology. We thank the International Space Science Institute (Bern) for hosting meetings of the international team on ‘Interpretation and modelling of SSI measurements’.

## References

- Arge, C. N., Hildner, E., Pizzo, V. J., Harvey, J. W., 2002. Two solar cycles of nonincreasing magnetic flux. *J. Geophys. Res.* 107 (A10), doi:10.1029/2001JA000503.
- Baliunas, S., Jastrow, R., 1990. Evidence for long-term brightness changes of solar-type stars. *Nature* 348, 520–523.
- Balmaceda, L., Krivova, N. A., Solanki, S. K., 2007. Reconstruction of solar irradiance using the Group sunspot number. *Adv. Space Res.* 40, 986–989.
- Balmaceda, L. A., Solanki, S. K., Krivova, N. A., Foster, S., 2009. A homogeneous sunspot areas database covering more than 130 years. *J. Geophys. Res.* 114, A07104, doi:10.1029/2009JA014299.

- Brasseur, G., Simon, P. C., 1981. Stratospheric chemical and thermal response to long-term variability in solar UV irradiance. *J. Geophys. Res.* 86, 7343–7362.
- Brueckner, G. E., Edlow, K. L., Floyd, L. E., Lean, J. L., Vanhoosier, M. E., 1993. The solar ultraviolet spectral irradiance monitor (SUSIM) experiment on board the Upper Atmosphere Research Satellite (UARS). *J. Geophys. Res.* 98, 10695–10711.
- Caccin, B., Ermolli, I., Fofi, M., Sambuco, A. M., 1998. Variations of the chromospheric network with the solar cycle. *Sol. Phys.* 177, 295–303.
- Camp, C. D., Tung, K. K., 2007. Surface warming by the solar cycle as revealed by the composite mean difference projection. *Geophys. Res. Lett.* 34, L14703, doi:10.1029/2007GL030207.
- Chapman, G. A., Cookson, A. M., Dobias, J. J., 1996. Variations in total solar irradiance during solar cycle 22. *J. Geophys. Res.* 101, 13541–13548.
- Crouch, A. D., Charbonneau, P., Beaubien, G., Paquin-Ricard, D., 2008. A model for the total solar irradiance based on active region decay. *Astrophys. J.* 677, 723–741.
- Danilović, S., Gandorfer, A., Lagg, A., Schüssler, M., Solanki, S. K., Vögler, A., Katsukawa, Y., Tsuneta, S., 2008. The intensity contrast of solar granulation: comparing Hinode SP results with MHD simulations. *Astron. Astrophys.* 484, L17–L20.

- Dewitte, S., Crommelynck, D., Mekaoui, S., Joukoff, A., 2004. Measurement and uncertainty of the long term total solar irradiance trend. *Sol. Phys.* 224, 209–216.
- Domingo, V., Ermolli, I., Fox, P., Fröhlich, C., Haberreiter, M., Krivova, N., Kopp, G., Schmutz, W., Solanki, S. K., Spruit, H. C., Unruh, Y., Vögler, 2009. Solar Surface Magnetism and Irradiance on Time Scales from Days to the 11-Year Cycle. *Space Sci. Rev.* 145, 337-380.
- Egorova, T., Rozanov, E., Manzini, E., Haberreiter, M., Schmutz, W., Zubov, V., Peter, T., 2004. Chemical and dynamical response to the 11-year variability of the solar irradiance simulated with a chemistry-climate model. *Geophys. Res. Lett.* 31, 6119–6122.
- Ermolli, I., Solanki, S. K., Tlatov, A. G., Krivova, N. A., Ulrich, R. K., Singh, J., 2009. Comparison among Ca II K spectroheliogram time series with an application to solar activity studies. *Astrophys. J.* 698, 1000–1009.
- Ermolli, I., Tlatov, A., Solanki, S. K., Krivova, N., Singh, J., 2007. Solar activity and irradiance studies with Ca II spectroheliograms: Potential and problems. In: Heinzl, P., Dorotovič, I., Rutten, J. (Eds.), "The Physics of Chromospheric Plasmas". *ASP Conf. Ser.* 368, 533–537.
- Fleming, E. L., Chandra, S., Jackman, C. H., Considine, D. B., Douglass, A. R., 1995. The middle atmospheric response to short and long term solar UV variations: analysis of observations and 2D model results. *J. Atmos. Terr. Phys.* 57, 333–365.

- Fligge, M., Solanki, S. K., Unruh, Y. C., 2000. Modelling irradiance variations from the surface distribution of the solar magnetic field. *Astron. Astrophys.* 353, 380–388.
- Fligge, M., Solanki, S. K., Unruh, Y. C., Fröhlich, C., Wehrli, C., 1998. A model of solar total and spectral irradiance variations. *Astron. Astrophys.* 335, 709–718.
- Floyd, L., Rottman, G., DeLand, M., Pap, J., 2003. 11 years of solar UV irradiance measurements from UARS. *ESA SP 535*, 195–203.
- Fontenla, J. M., Avrett, E. H., Loeser, R., 1993. Energy balance in the solar transition region. III - Helium emission in hydrostatic, constant-abundance models with diffusion. *Astrophys. J.* 406, 319–345.
- Fontenla, J. M., Harder, J., Rottman, G., Woods, T. N., Lawrence, G. M., Davis, S., 2004. The signature of solar activity in the infrared spectral irradiance. *Astrophys. J. Lett.* 605, L85–L88.
- Foster, S., 2004. Reconstruction of Solar Irradiance Variations for use in Studies of Global Climate Change: Application of Recent SOHO Observations with Historic Data from the Greenwich Observatory. Ph.D. thesis, University of Southampton, School of Physics and Astronomy.
- Foukal, P., 1996. The behavior of solar magnetic plages measured from Mt. Wilson observations between 1915-1984. *Geophys. Res. Lett.* 23, 2169–2172.
- Frederick, J. E., 1977. Chemical response of the middle atmosphere to changes in the ultraviolet solar flux. *Planet. Space Sci.* 25, 1–4.

- Fröhlich, C., 2006. Solar irradiance variability since 1978: Revision of the PMOD composite during solar cycle 21. *Space Sci. Rev.* 125, 53–65.
- Fröhlich, C., Andersen, B., Appourchaux, T., Berthomieu, G., Crommelynck, D. A., Domingo, V., Fichot, A., Finsterle, W., Gomez, M. F., Gough, D., Jimenez, A., Leifsen, T., Lombaerts, M., Pap, J. M., Provost, J., Cortes, T. R., Romero, J., Roth, H., Sekii, T., Telljohann, U., Toutain, T., Wehrli, C., 1997. First Results from VIRGO, the Experiment for Helioseismology and Solar Irradiance Monitoring on SOHO. *Sol. Phys.* 170, 1–25.
- Haigh, J. D., 1994. The role of stratospheric ozone in modulating the solar radiative forcing of climate. *Nature* 370, 544–546.
- Haigh, J. D., 1999. Modelling the impact of solar variability on climate. *J. Sol. Atm. Terr. Phys.* 61, 63–72.
- Haigh, J. D., 2007. The Sun and the Earth’s Climate. *Liv. Rev. Sol. Phys.* <http://solarphysics.livingreviews.org/Articles/lrsp-2007-2/>.
- Harder, J., Lawrence, G., Fontenla, J., Rottman, G., Woods, T., 2005. The Spectral Irradiance Monitor: Scientific Requirements, Instrument Design, and Operation Modes. *Sol. Phys.* 230, 141–167.
- Harder, J. W., Fontenla, J. M., Pilewskie, P., Richard, E. C., Woods, T. N., 2009. Trends in solar spectral irradiance variability in the visible and infrared. *Geophys. Res. Lett.* 36, doi:10.1029/2008GL036797.
- Heath, D. F., Schlesinger, B. M., 1986. The Mg 280-nm doublet as a monitor of changes in solar ultraviolet irradiance. *J. Geophys. Res.* 91, 8672–8682.

- Hickey, J. R., Stowe, L. L., Jacobowitz, H., Pellegrino, P., Maschhoff, R. H., House, F., Vonder Haar, T. H., 1980. Initial solar irradiance determinations from Nimbus 7 cavity radiometer measurements. *Science* 208, 281–283.
- Hirzberger, J., Bonet, J. A., Vázquez, M., Hanslmeier, A., 1999. Time Series of Solar Granulation Images. II. Evolution of Individual Granules. *Astrophys. J.* 515, 441–454.
- Hudson, H. S., Silva, S., Woodard, M., Willson, R. C., 1982. The effects of sunspots on solar irradiance. *Sol. Phys.* 76, 211–219.
- Jones, H. P., Duvall, T. L., Harvey, J. W., Mahaffey, C. T., Schwitters, J. D., Simmons, J. E., 1992. The NASA/NSO spectromagnetograph. *Sol. Phys.* 139, 211–232.
- Kariyappa, R., Pap, J. M., 1996. Contribution of chromospheric features to UV irradiance variability from spatially-resolved Ca II K spectroheliograms. *Sol. Phys.* 167, 115–123.
- Kopp, G., Lawrence, G., 2005. The total irradiance monitor (tim): Instrument design. *Sol. Phys.* 230, 91–109.
- Kopp, G., Lawrence, G., Rottman, G., 2005. The Total Irradiance Monitor (TIM): Science Results. *Sol. Phys.* 230, 129–139.  
URL <http://adsabs.harvard.edu/abs/2005SoPh..230..129K>
- Krivova, N. A., Balmaceda, L., Solanki, S. K., 2007. Reconstruction of solar total irradiance since 1700 from the surface magnetic flux. *Astron. Astrophys.* 467, 335–346.

- Krivova, N. A., Solanki, S. K., 2005. Reconstruction of solar UV irradiance. *Adv. Space Res.* 35, 361–364.
- Krivova, N. A., Solanki, S. K., Fligge, M., Unruh, Y. C., 2003. Reconstruction of solar total and spectral irradiance variations in cycle 23: is solar surface magnetism the cause? *Astron. Astrophys.* 399, L1–L4.
- Krivova, N. A., Solanki, S. K., Floyd, L., 2006. Reconstruction of solar UV irradiance in cycle 23. *Astron. Astrophys.* 452, 631–639.
- Krivova, N. A., Solanki, S. K., Wenzler, T., 2009a. ACRIM-gap and total solar irradiance revisited: Is there a secular trend between 1986 and 1996? *Geophys. Res. Lett.* 36, L20101, doi:10.1029/2009GL040707.
- Krivova, N. A., Solanki, S. K., Wenzler, T., Podlipnik, B., 2009b. Reconstruction of solar UV irradiance since 1974. *J. Geophys. Res.* 114, D00I04, doi:10.1029/2009JD012375.
- Krivsky, L., 1984. Long-term fluctuations of solar activity during the last thousand years. *Sol. Phys.* 93, 189–194.
- Kurucz, R., 1993. ATLAS9 Stellar Atmosphere Programs and 2 km/s grid. ATLAS9 Stellar Atmosphere Programs and 2 km/s grid. Kurucz CD-ROM No. 13. Cambridge, Mass.: Smithsonian Astrophysical Observatory, 1993. 13.
- Kurucz, R. L., 1992. Finding the 'Missing' solar ultraviolet opacity. *Revista Mexicana de Astronomia y Astrofisica* 23, 181–186.

- Kurucz, R. L., 2005. ATLAS12, SYNTHE, ATLAS9, WIDTH9, et cetera. Mem. Soc. Astron. It. Suppl. 8, 14–24.
- Langematz, U., Matthes, K., Grenfell, J. L., 2005. Solar impact on climate: modeling the coupling between the middle and the lower atmosphere. Mem. Soc. Astron. It. 76, 868–875.
- Lean, J., Beer, J., Bradley, R., 1995. Reconstruction of solar irradiance since 1610: Implications for climate change. Geophys. Res. Lett. 22, 3195–3198.
- Lee, III, R. B., Gibson, M. A., Wilson, R. S., Thomas, S., 1995. Long-term total solar irradiance variability during sunspot cycle 22. J. Geophys. Res. 100, 1667–1675.
- Livingston, W. C., Harvey, J., Slaughter, C., Trumbo, D., 1976. Solar magnetograph employing integrated diode arrays. Appl. Opt. 15, 40–52.
- Lockwood, M., 2005. Solar outputs, their variations and their effects on Earth. In: Rüedi, I., Güdel, M., Schmutz, W. (Eds.), The Sun, Solar Analogs and the Climate, 34th ‘Saas Fee’ Advanced Course. Springer, Berlin, pp. 109–306.
- Lockwood, M., Rouillard, A. P., Finch, I. D., 2009. The Rise and Fall of Open Solar Flux During the Current Grand Solar Maximum. Astrophys. J. 700, 937–944.
- Lockwood, M., Stamper, R., Wild, M. N., 1999. A doubling of the Sun’s coronal magnetic field during the last 100 years. Nature 399, 437–439.



- Ortiz, A., Solanki, S. K., Domingo, V., Fligge, M., Sanahuja, B., 2002. On the intensity contrast of solar photospheric faculae: and network elements. *Astron. Astrophys.* 388, 1036–1047.
- Pagaran, J., Weber, M., Burrows, J., 2009. Solar Variability from 240 to 1750 nm in Terms of Faculae Brightening and Sunspot Darkening from SCIAMACHY. *Astrophys. J.* 700, 1884–1895.
- Rottman, G., 2005. The SORCE Mission. *Sol. Phys.* 230, 7–25.
- Rottman, G. J., Woods, T. N., Sparn, T. P., 1993. Solar-Stellar Irradiance Comparison Experiment. I - Instrument design and operation. *J. Geophys. Res.* 98 (D6), 10667–10677.
- Rozanov, E., Egorova, T., Schmutz, W., Peter, T., 2006. Simulation of the stratospheric ozone and temperature response to the solar irradiance variability during sun rotation cycle. *J. Atm. Sol.-Terr. Phys.* 68, 2203–2213.
- Scafetta, N., Willson, R. C., 2009. ACRIM-gap and TSI trend issue resolved using a surface magnetic flux TSI proxy model. *Geophys. Res. Lett.* 36, L05701, doi:10.1029/2008GL036307.
- Scherrer, P. H., Bogart, R. S., Bush, R. I., Hoeksema, J. T., Kosovichev, A. G., Schou, J., Rosenberg, W., Springer, L., Tarbell, T. D., Title, A., Wolfson, C. J., Zayer, I., MDI Engineering Team, 1995. The Solar Oscillations Investigation - Michelson Doppler Imager. *Sol. Phys.* 162, 129–188.
- Schove, D. J., 1955. The Sunspot Cycle, 649 BC to AD 2000. *J. Geophys. Res.* 60, 127–146.

- Siscoe, G. L., 1980. Evidence in the auroral record for secular solar variability. *Rev. Geophys. Sp. Phys.* 18, 647–658.
- Skupin, J., Noël, S., Wuttke, M. W., Gottwald, M., Bovensmann, H., Weber, M., Burrows, J. P., 2005. SCIAMACHY solar irradiance observation in the spectral range from 240 to 2380 nm. *Adv. Space Res.* 35, 370–375.
- Snow, M., McClintock, W. E., Rottman, G., Woods, T. N., 2005. Solar Stellar Irradiance Comparison Experiment II (SOLSTICE II): Examination of the solar stellar comparison technique. *Sol. Phys.* 230, 295–324.
- Solanki, S. K., 1986. Velocities in solar magnetic flux tubes. *Astron. Astrophys.* 168, 311–329.
- Solanki, S. K., 1993. Smallscale Solar Magnetic Fields - an Overview. *Space Sci. Rev.* 63, 1–2.
- Solanki, S. K., Schüssler, M., Fligge, M., 2000. Evolution of the Sun's large-scale magnetic field since the Maunder minimum. *Nature* 408, 445–447.
- Solanki, S. K., Schüssler, M., Fligge, M., 2002. Secular variation of the Sun's magnetic flux. *Astron. Astrophys.* 383, 706–712.
- Solanki, S. K., Seleznyov, A. D., Krivova, N. A., 2003. Solar irradiance fluctuations on short timescales. *ESA SP 535*, 285–588.
- Solanki, S. K., Unruh, Y. C., 1998. A model of the wavelength dependence of solar irradiance variations. *Astron. Astrophys.* 329, 747–753.

- Solanki, S. K., Usoskin, I. G., Kromer, B., Schüssler, M., Beer, J., 2004. Unusual activity of the Sun during recent decades compared to the previous 11,000 years. *Nature* 431, 1084–1087.
- Tanaka, H., Castelli, J. P., Covington, A. E., Krüger, A., Landecker, T. L., Tlamicha, A., 1973. Absolute Calibration of Solar Radio Flux Density in the Microwave Region. *Sol. Phys.* 29, 243–262.
- Thuillier, G., Foujols, T., Bolsée, D., Gillotay, D., Hersé, M., Peetermans, W., Decuyper, W., Mandel, H., Sperfeld, P., Pape, S., Taubert, D. R., Hartmann, J., 2009. SOLAR/SOLSPEC: Scientific objectives, instrument performance and its absolute calibration using a blackbody as primary standard source. *Sol. Phys.* 257, 185–213.
- Tlatov, A. G., Pevtsov, A. A., Singh, J., 2009. A new method of calibration of photographic plates from three historic data sets. *Sol. Phys.* 255, 239–251.
- Topka, K. P., Tarbell, T. D., Title, A. M., 1997. Properties of the smallest solar magnetic elements. II. Observations versus Hot Wall models of faculae. *Astrophys. J.* 484, 479.
- Unruh, Y. C., Krivova, N. A., Solanki, S. K., Harder, J. W., Kopp, G., 2008. Spectral irradiance variations: comparison between observations and the SATIRE model on solar rotation time scales. *Astron. Astrophys.* 486, 311–323.
- Unruh, Y. C., Solanki, S. K., Fligge, M., 1999. The spectral dependence of facular contrast and solar irradiance variations. *Astron. Astrophys.* 345, 635–642.

- Unruh, Y. C., Solanki, S. K., Schüssler, M., Vögler, A., Garcia-Alvarez, D., 2009. Towards long-term solar irradiance modelling: Network contrasts from magneto-convection simulations. In: Stempels, E. (Ed.), ASP Conf. Ser. Vol. 1094. pp. 768–771.
- Usoskin, I. G., Mursula, K., Solanki, S., Schüssler, M., Alanko, K., 2004. Reconstruction of solar activity for the last millennium using  $^{10}\text{Be}$  data. *Astron. Astrophys.* 413, 745–751.
- Usoskin, I. G., Solanki, S. K., Korte, M., 2006. Solar activity reconstructed over the last 7000 years: The influence of geomagnetic field changes. *Geophys. Res. Lett.* 33, L08103, doi:10.1029/2006GL025921.
- Usoskin, I. G., Solanki, S. K., Kovaltsov, G. A., 2007. Grand minima and maxima of solar activity: new observational constraints. *Astron. Astrophys.* 471, 301–309.
- Viereck, R. A., Floyd, L. E., Crane, P. C., Woods, T. N., Knapp, B. G., Rottman, G., Weber, M., Puga, L. C., DeLand, M. T., 2004. A composite Mg II index spanning from 1978 to 2003. *Space Weather* 2, doi:10.1029/2004SW000084.
- Viereck, R. A., Puga, L. C., 1999. The NOAA Mg II core-to-wing solar index: Construction of a 20-year time series of chromospheric variability from multiple satellites. *J. Geophys. Res.* 104, 9995–10006.
- Vögler, A., Shelyag, S., Schüssler, M., Cattaneo, F., Emonet, T., Linde, T., 2005. Simulations of magneto-convection in the solar photosphere. *Equa-*

- tions, methods, and results of the MURaM code. *Astron. Astrophys.* 429, 335–351.
- Wang, Y.-M., Lean, J. L., Sheeley, N. R., 2005. Modeling the Sun’s magnetic field and irradiance since 1713. *Astrophys. J.* 625, 522–538.
- Wenzler, T., 2005. Reconstruction of solar irradiance variations in cycles 21–23 based on surface magnetic fields. Ph.D. thesis, ETH Zürich.
- Wenzler, T., Solanki, S. K., Krivova, N. A., 2005. Can surface magnetic fields reproduce solar irradiance variations in cycles 22 and 23? *Astron. Astrophys.* 432, 1057–1061.
- Wenzler, T., Solanki, S. K., Krivova, N. A., 2009. Reconstructed and measured total solar irradiance: Is there a secular trend between 1978 and 2003? *Geophys. Res. Lett.* 36, L11102, doi:10.1029/2009GL037519.
- Wenzler, T., Solanki, S. K., Krivova, N. A., Fluri, D. M., 2004. Comparison between KPVT/SPM and SoHO/MDI magnetograms with an application to solar irradiance reconstructions. *Astron. Astrophys.* 427, 1031–1043.
- Wenzler, T., Solanki, S. K., Krivova, N. A., Fröhlich, C., 2006. Reconstruction of solar irradiance variations in cycles 21–23 based on surface magnetic fields. *Astron. Astrophys.* 460, 583–595.
- White, O. R., Skumanich, A., Lean, J., Livingston, W. C., Keil, S. L., 1992. The sun in a noncycling state. *Publ. Astron. Soc. Pac.* 104, 1139–1143.
- Willson, R. C., 1994. Irradiance observations of SMM, Spacelab 1, UARS and ATLAS experiments. In: Pap, J. M., Fröhlich, C., Hudson, H. S., Solanki,

- S. K. (Eds.), *The Sun as a Variable Star: Solar and Stellar Irradiance Variations*. Cambridge Univ. Press, Cambridge, pp. 54–62.
- Willson, R. C., Gulkis, S., Janssen, M., Hudson, H. S., Chapman, G. A., 1981. Observations of solar irradiance variability. *Science* 211, 700–702.
- Willson, R. C., Mordvinov, A. V., 2003. Secular total solar irradiance trend during solar cycles 21–23. *Geophys. Res. Lett.* 30, 1199, doi:10.1029/2002GL016038.
- Wilson, R. C., 2001. The ACRIMSAT/ACRIM3 experiment — Extending the precision, long-term total solar irradiance climate database. *The Earth Observer* 13, 14–17.
- Woods, T. N., 2008. Recent advances in observations and modeling of the solar ultraviolet and X-ray spectral irradiance. *Adv. Sp. Res.* 42, 895–902.
- Woods, T. N., Tobiska, W. K., Rottman, G. J., Worden, J. R., 2000. Improved solar Lyman- $\alpha$  irradiance modeling from 1947 through 1999 based on UARS observations. *JGR* 105 (A12), 27195–27215.
- Worden, J. R., White, O. R., Woods, T. N., 1998. Evolution of chromospheric structures derived from Ca II K spectroheliograms: Implications for solar ultraviolet irradiance variability. *Astrophys. J.* 496, 998–1014.
- Zwaan, C., 1978. On the Appearance of Magnetic Flux in the Solar Photosphere. *Sol. Phys.* 60, 213–240.